PNAS RESEARCH ARTICLE | IMMUNOLOGY AND INFLAMMATION

Lymph node stromal cell responses to perinatal T cell waves, a temporal atlas

Teshika Jayewickreme[a], Christophe Benoist[a], and Diane Mathis[a,1]

Contributed by Diane Mathis; received September 29, 2023; accepted October 30, 2023; reviewed by Bernard Malissen and Jeffrey V. Ravetch

The perinatal period is a critical time window in establishing T cell tolerance. Regulatory T cells (Tregs) made during the first 2 wk of life are key drivers of perinatal tolerance induction, but how these cells are generated and operate has not been established. To elucidate the unique environment murine perinatal Tregs encounter within the lymph nodes (LNs) as they first emerge from the thymus, and how it evolves over the succeeding days, we employed single-cell RNA sequencing to generate an atlas of the early LN niche. A highly dynamic picture emerged, the stromal cell compartment showing the most striking changes and putative interactions with other LN cell compartments. In particular, LN stromal cells showed increasing potential for lymphocyte interactions with age. Analogous studies on mice lacking α:β T cells or enriched for autoreactive α:β T cells revealed an acute stromal cell response to α:β T cell dysfunction, largely reflecting dysregulation of Tregs. Punctual ablation of perinatal Tregs induced stromal cell activation that was dependent on both interferon-gamma signaling and activation of conventional CD4$^+$ T cells. These findings elucidate some of the earliest cellular and molecular events in perinatal induction of T cell tolerance, providing a framework for future explorations.

T cell | regulatory T cell | neonatal | interferon

A fundamental challenge for the adaptive immune system is establishing a T cell repertoire that is broad enough to recognize the universe of foreign pathogens but is specific enough to minimize responses to self-antigens. The mammalian immune system has evolved multiple complementary layers of protection to solve this problem. As a first line of defense, thymocytes receiving a strong signal through their T cell receptors (TCRs) are deleted from the differentiating T cell pool; yet this process of thymic clonal deletion is incomplete (1). As a restraint on the self-reactive T cells that escape into the periphery, a subset of moderately reactive thymocytes differentiate into Foxp3$^+$CD4$^+$ regulatory T cells (Tregs) that actively suppress self-specific T cells in both lymphoid organs and nonlymphoid tissues (2). A multitude of additional layers of peripheral tolerance mechanisms work in concert with Tregs, such as antigenic ignorance and anergy induction (3–5).

A too often-overlooked aspect in the study of immunological tolerance is the importance of tolerizing events during early life. Hints of a perinatal tolerance window first arose through experiments on cattle as early as the 1940s and later on rodents, showing that perinatal inoculation with allogenic antigens could prevent rejection to allografts in adulthood (6). While these findings proved prescient for the burgeoning field of immunology, much debate ensued as to the mechanisms involved. One set of models suggested that perinatal tolerance stemmed from some intrinsic quality of the perinatal T cells: for example, their immature state might compromise their ability to clear antigen, thereby fostering tolerance rather than immunity (7–10). Yet a wave of studies in the 1990s showed that the apparent effectiveness of perinatal tolerization might be explained at least partly by differences in inoculum dose, inflammatory mediators, or antigen-presenting cell (APC) composition (8, 11, 12).

While these models grappled with explaining tolerance to exogenous antigens, a parallel line of work that modeled loss of T cell tolerance to endogenous self-antigens in thymectomized mice continued to show that the perinatal period is crucial for T cell tolerance induction (13). Later findings on Aire—a stromal cell transcription factor (TF) that facilitates exposure of thymocytes to peripheral tissue antigens, thereby driving thymic tolerance induction (14)—provided further strong evidence for the importance of the perinatal window. Studies on transgenic mice with inducible Aire expression revealed it to be dispensable after the first 2 wk of life (15). Furthermore, transfer experiments showed that perinatally tagged but not adult-tagged Tregs are necessary and sufficient to counter the tissue-specific autoimmunity characteristic of mice lacking Aire (16). Together, these observations highlighted the first 2 wk of life as a pivotal time window for the development of long-lived tissue tolerance.

Significance

Early life poses the challenge of establishing an immune system tolerant to self while still maintaining sensitivity to pathogens. Generation of a special wave of Foxp3+CD4+ regulatory T (Treg) cells during the first weeks of life is an important part of the strategy to meet this challenge. Little is known about how these cells are generated and maintain tolerance. Exploring the early lymph node environment, via temporally resolved, whole-tissue, single-cell RNA sequencing, we identified stromal cells as the most distinctive cell compartment perinatal Tregs encountered. Studies on T cell–deficient mice and mice enriched in autoreactive T cells revealed a role for perinatal Tregs in maintaining early stromal cell homeostasis largely, but not entirely, through control of local interferon responses.

Author affiliations: [a]Department of Immunology, Harvard Medical School, Boston, MA 02115

Author contributions: T.J. and D.M. designed research; T.J. performed research; T.J. analyzed data; T.J. edited the paper; C.B. edited the paper and supervised; D.M. edited the paper, supervised, and acquired funding; and T.J., C.B., and D.M. wrote the paper.

Reviewers: B.M., Centre d'Immunologie de Marseille-Luminy; and J.V.R., The Rockefeller University.

The authors declare no competing interest.

[1]To whom correspondence may be addressed. Email: dm@hms.harvard.edu.

This article contains supporting information online at https://www.pnas.org/lookup/suppl/doi:10.1073/pnas.2316957120/-/DCSupplemental.

Published December 11, 2023.

T cell–intrinsic explanations for the protective role of perinatal Tregs have been proposed. Early-life thymocytes display a less diverse, more germline-encoded TCR repertoire than do older mice due to delayed expression of terminal deoxynucleotidyl transferase (TdT), the enzyme responsible for insertion of random nucleotides during *Tra/b* gene assembly (17, 18). Consequently, neonatal mice have a less diverse, more cross-reactive T cell repertoire (17, 19). Likewise, ontogenetic differences between hematopoietic cell progenitors from the fetal liver versus bone marrow may explain variations in epigenetic profiles and differentiation potentials in perinates versus adults (20–22). Once they emerge from the thymus, perinatal T cells are confronted with a distinct environment in secondary lymphoid organs or within a diversity of nonlymphoid tissues, which may predicate differential priming, proliferation, or cellular cross talk vis-a-vis newly emergent adult T cells (23–26).

What is the lymphoid-organ environment T cells first encounter when they exit the thymus in perinatal mice? And how does this environment evolve over the initial 2 wk of life? A single-cell RNA sequencing (scRNAseq) atlas of lymph nodes (LNs) across this early time window allowed us to capture the heterogeneity of the entire niche, identifying stromal cells as the most transcriptionally divergent compartment. Stromal cells showed an acute transcriptional sensitivity to dysregulation of the T cell compartment, at least partially attributable to dysregulation of interferon expression by T and other cells.

Results

scRNAseq Atlas of the Murine Early LN Niche. For an unbiased view of the perinatal LN niche, in particular how its components change over time, we performed scRNAseq on peripheral LNs (pooled inguinal, axillary, and brachial) from early perinatal [Day (D)4-6], late perinatal (D12-15) and young adult (D30-45) female C57BL/6 (B6) mice. These ages represent key points during the early life of the mouse. The early perinatal period encompasses the arrival of the first waves of αβ T (Tαβ) cells in the peripheral LNs and is especially important for generating Tregs that protect Aire-deficient mice from multiorgan autoimmunity (15, 16). The late perinatal period marks the end of the Aire-dependent perinatal window of tolerization, and coincides with contraction and anergization of the first waves of T cells that become activated and proliferate in the periphery (27). Young adulthood marks a period wherein newly generated Tregs are insufficient to counteract the autoimmunity associated with Aire deficiency. Skin-draining LNs were chosen to minimize potential covariates due to gut microbiota colonization and transitions in the perinatal diet. Independent duplicate samples from each age were hashtagged, were sorted on the basis of CD45 expression (*SI Appendix*, Fig. S1*A*), and all cells from each replicate were encapsulated together to minimize batch effects and to balance RNA capture between the hematopoietic and nonhematopoietic compartments. After preprocessing and merging the replicates' data across the entire age range, data from 24,402 cells were retained with an average of 1,300 genes per cell. Clustering, visualized by Uniform Manifold Approximation and Projection (UMAP), revealed the expected extensive heterogeneity (Fig. 1*A*). Cell-type classification was conducted using the SingleR package, correlating cell clusters with cell-type signatures found in the Immgen database (https://www.immgen.org) as well as expression levels of key lineage-defining genes. This age-spanning UMAP served as an atlas for exploring the LN environment when T cells first arrive and how it evolves over early life.

Distillation of the data from each age (Fig. 1*B*) revealed that the D5 perinatal LN niche already contained all major innate and adaptive immunocyte types known to reside in the adult LN, including difficult-to-characterize types such as innate lymphoid cells (ILCs) and recently discovered, rare types like *Aire*-expressing APCs (28). They also contained all of the major nonhematopoietic lineages, such as blood endothelial cells, lymphatic endothelial cells, and fibroblastic reticular cells (FRCs). To visualize cellular dynamics over time, we plotted the density of cell states within the UMAP of each age (Fig. 1*C*) and also plotted the density differentials between successive ages (Fig. 1*D*). While all populations showed some transcriptional shifts over time, the most profound alterations occurred in the stromal cell clusters, especially FRCs. More modest shifts in myeloid APCs and cycling T and B cells were also evident. Histograms of fractional representations quantified and confirmed these observations (Fig. 1*E*). Moreover, in age comparisons, FRCs consistently had the most differentially expressed genes (*SI Appendix*, Fig. S1*B*). Given the dramatic changes that occurred during the first 2 wk of life, and the importance of this window for perinatal tolerance induction, we focused our downstream explorations on D5 and W2.

Leveraging the transcriptomic data of all LN populations across the perinatal window, we used CellChat (29) to predict putative interactions across the major cell types. On D5, as the first lymphocytes are immigrating to the LN, FRCs were the strongest putative interaction partners, forming a prominent network with APCs, Tαβ cells and B cells (Fig. 1*F*). The magnitude of incoming versus outgoing interactions indicated that the majority of the putative outgoing interactions emanated from FRCs and were directed to all three of the other compartments (Fig. 1*G*). By W2 the putative network shifted more toward APC: Tαβ cell interactions (Fig. 1 *H* and *I*). While FRCs continued to provide outgoing interaction signals, other populations, such as APCs and B cells, increased their outgoing signals: Tαβ cells remained the predominate signal receivers. Concerning individual putative interaction pairs, expression of chemokine genes (*Ccl21a, Ccl19, Ccl2,* and *App*) and growth factors (*Ptn* and *Mdk*) in FRCs drove outgoing interactions, putatively inciting recruitment of T, B, and myeloid cells (*SI Appendix*, Fig. S1*C*). Outgoing signals from T cells were relatively sparse (*SI Appendix*, Fig. S1*D*).

LN Stromal Cell Dynamics. Distillation of the FRCs from the two perinatal time points revealed almost no overlap in the D5 and W2 UMAP representations (Fig. 2*A*). Nonetheless, reclustering (Fig. 2*B*) and analysis of the expression patterns of key marker genes (Fig. 2*C*) permitted us to delineate previously reported FRC subtypes (25, 30). According to the fractional representations of the various FRC subtypes, the most substantial changes between D5 and W2 were the appearance of a *Cxcl12*$^+$ subtype accompanied by decreases in the *Ccl19*$^+$, *Cd34*$^+$ and cycling subtypes (Fig. 2*D*). RNA-velocity analysis predicted that cells from the cycling cluster gave rise to cells in the *Ccl19*$^+$ cluster, which engendered cells in the *Cxcl12*$^+$ cluster (Fig. 2*E*). The D5 and W2 FRC compartments both contained pools of *Cd34*$^+$ stromal cell progenitors predicted to directly seed the perivascular cell subtype and to give rise to the three other FRC subtypes either directly or indirectly. Both population-level RNAseq comparison (Fig. 2*F*) and Gene Set Enrichment Analysis (GSEA) (Fig. 2*G*) of D5 vs. W2 FRCs corroborated the early enrichment of dividing cells. Furthermore, as the stromal cells differentiated across the perinatal period, they acquired increased expression of transcripts encoding trophic factors for other key LN cell compartments, like *Il7* and *Tnfsf13b* for lymphocytes and *Ccl9* and *Flt3l* for myeloid cells (Fig. 2*F*). In short, then, the stromal compartment of D5 LNs was impoverished in trophic-factor transcripts and cell subtypes found at W2 or, as previously reported, in adults (25, 31).

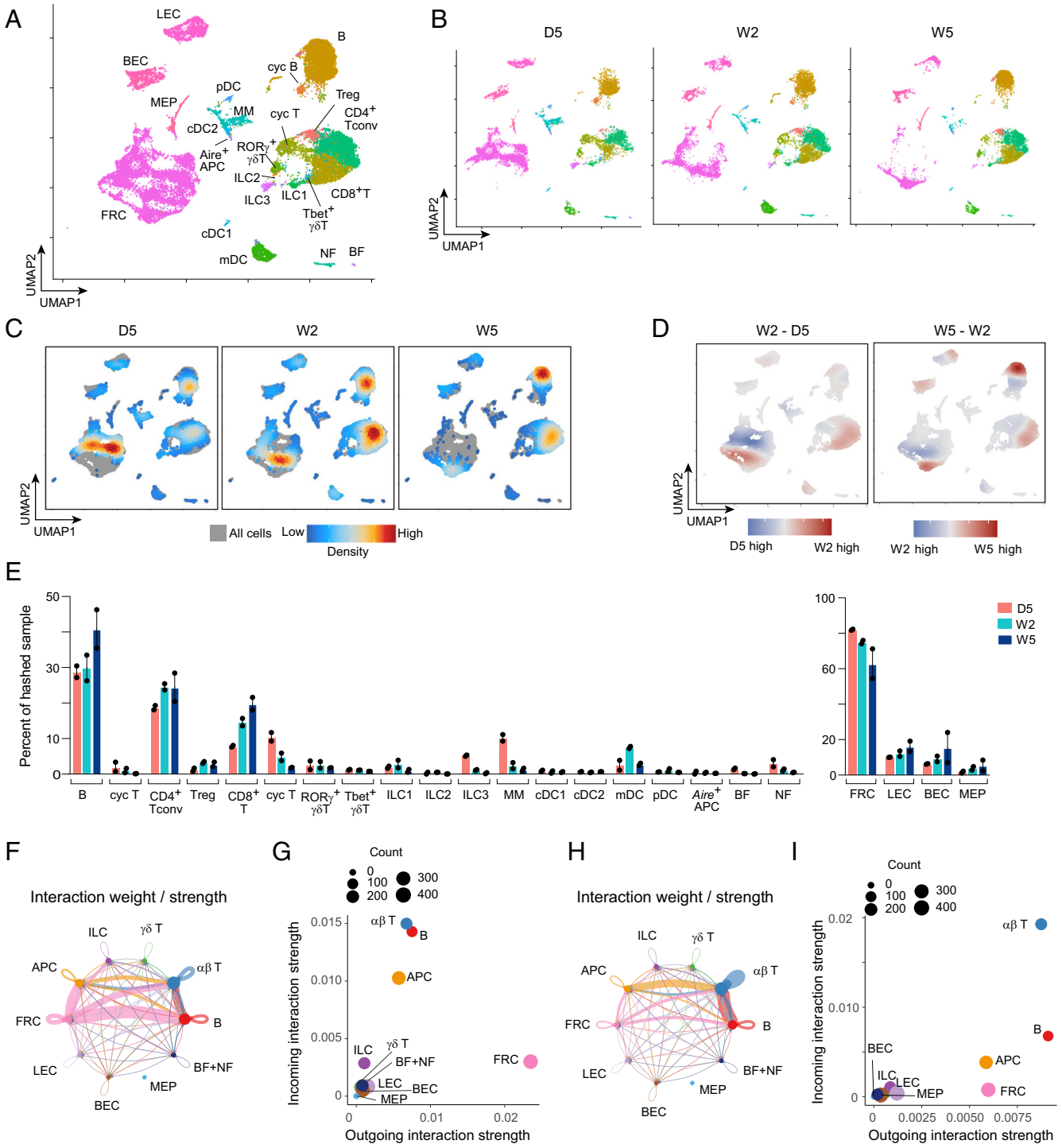

Fig. 1. Lymph node niche across the early life of the mouse. (*A*) UMAP plot of scRNAseq of LN cells combined from day 5 (D5), week 2 (W2), and week 5 (W5). (*B*) UMAP plots as in *A*, split by age. (*C*) Local cell densities on the UMAP space. (*D*) UMAP density differential plots. Dots colored by the difference in 2-dimensional densities between the ages in comparison, scaled to maximum and minimum values across both panels. (*E*) Histograms representing the proportion of each cell type cluster per age, (*Left*) CD45+ hematopoietic cells and (*Right*) CD45- stromal cells. (*F*) Circle plot showing the inferred interaction network weights among the different cell types at D5 calculated by CellChat. Each dot and line is colored by cell type and the line thickness is representative of relative interaction probability. (*G*) Scatterplot comparing the outgoing and incoming interaction strengths for D5. Each dot is colored by cell type and size proportional to the total number of inferred links. (*H*) Circle plot as in *F* for W2. (*I*) Scatterplot as in *G* for W2. UMAP, Uniform manifold approximation and projection; Cyc, cycling cells, FRC, fibroblastic reticular cell; BEC, blood endothelial cell; LEC, lymphatic endothelial cell; MEP, megakaryocytic-erythroid progenitors; Tconv, T conventional cells; Treg, regulatory T cells; ILC, innate lymphoid cell; MM, monocyte–macrophage; cDC, conventional dendritic cell; mDC, migratory dendritic cell; APC, antigen-presenting cell; NF, neutrophil; BF, basophil.

APC Heterogeneity in the Perinatal LN. APCs are essential for T cell priming within the LN. In the adult mouse, professional APCs such as DCs work in concert with the LN stromal cell network to efficiently prime naive T cells (32). To explore the evolution of APC compartments during the perinatal time window, we distilled the D5 and W2 myeloid populations from the data illustrated in Fig. 1*A* and reclustered them in isolation (Fig. 3*A*). Expression of lineage-defining marker transcripts (Fig. 3*B*) as well as Immgen myeloid cell signatures (https://www.immgen.org) allowed us to identify known myeloid cell types (Fig. 3*A*). In addition to the

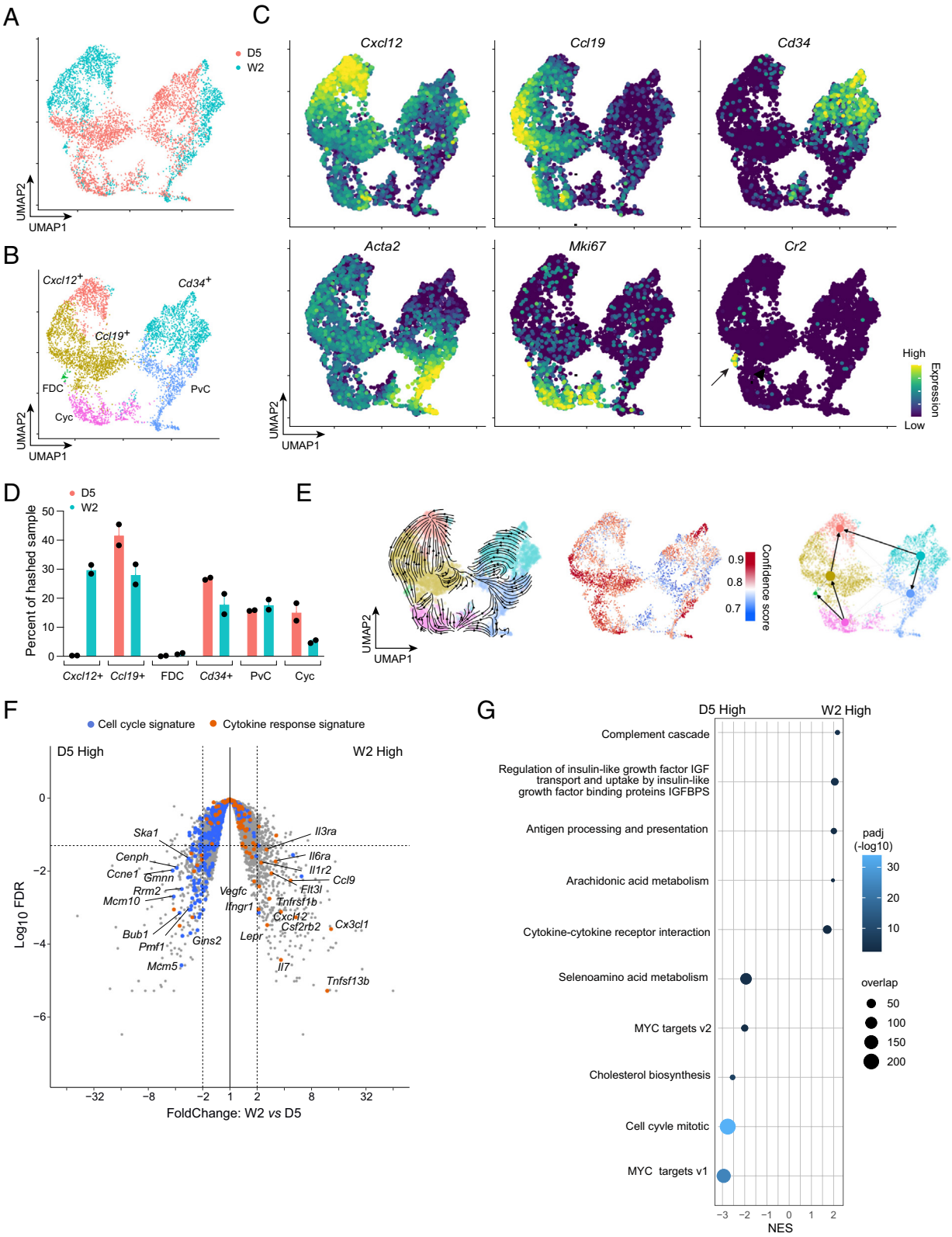

Fig. 2. Stromal cell heterogeneity across the perinatal period. (*A*) UMAP plot of D5 and W2 FRCs. (*B*) UMAP plot as in *A* colored by the stromal subpopulation clusters. (*C*) UMAP plot as in *A* colored by the scaled expression of each indicated gene. (*D*) Proportions of each stromal subpopulation per condition. (*E*) Velocity trajectory analysis, (*Left*) summarized velocity vector field, (*Middle*) PAGA of the velocity trajectories across clusters, and (*Right*) velocity vector field coherence (confidence). (*F*) Volcano plots from W2 vs. D5 FRCs with highlighted gene signatures for "Cell Cycle" (blue) and "Cytokine-cytokine receptor interaction" (orange). Five replicates for W2, four replicates for D5. (*G*) Relevant GSEA plots comparing differentially expressed FRC transcripts W2 vs. D5. Abbreviations as in Fig. 1.

commonly annotated LN APC populations, such as migratory DCs (mDCs), conventional DCs (cDC1s, cDC2s), plasmacytoid DCs (pDCs), monocytes/macrophages (MMs), neutrophils (NFs), and basophils (BFs), we also identified a rare cluster alongside mDCs that expressed *Aire* (designated *Aire*$^+$ APCs). While Aire is highly preferentially expressed in medullary thymic epithelial cells,

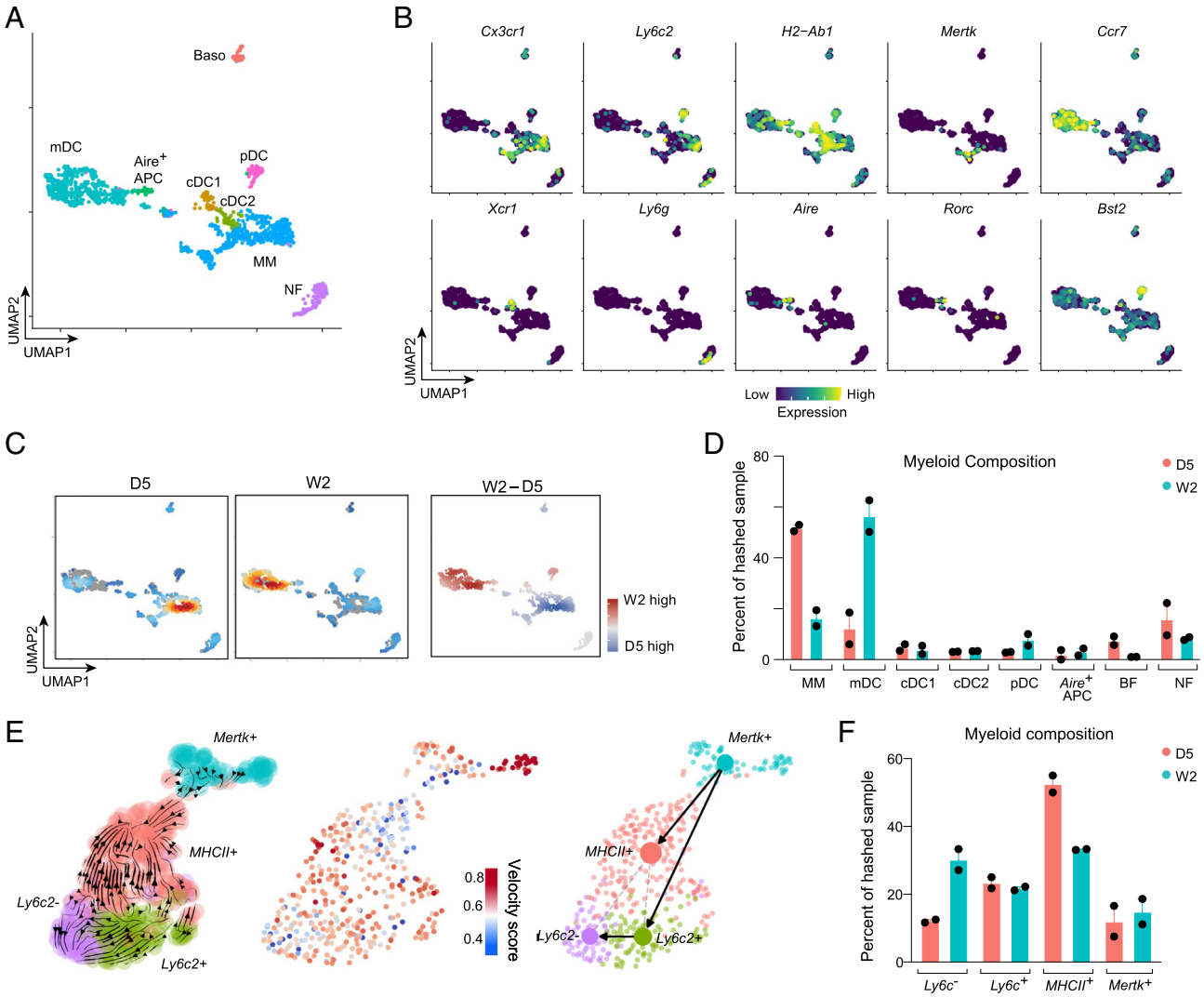

Fig. 3. Temporal shifts in myeloid cell populations. (*A*) UMAP plot of D5 and W2 myeloid populations. (*B*) UMAP plot as in *A* colored by the scaled expression of each indicated gene. (*C*) Local cell densities of (*Left*) D5, (*Middle*) W2, and (*Right*) density differential. (*D*) Proportion of subtype cluster per age. (*E*) Velocity trajectory analysis of MM subtypes, plotted as in Fig. 2. (*F*) Proportion of each MM subtype cluster per age. Abbreviations as in Fig. 1.

extrathymic transcription has been observed in DCs, ILC3s, and/or stromal cells and has been implicated in deletional tolerance and peripheral Treg induction during early life (28). Our data captured an *Aire*$^+$ APC population that clustered with the mDCs (Figs. 1*A* and 3*A*).

Broad analysis of the major myeloid APC populations across the two time points showed a shift from MM preponderance at D5 to mDC dominance at W2 (Fig. 3 *C* and *D*), which we confirmed by flow cytometry (*SI Appendix*, Fig. S3*A*, gating schema in *SI Appendix*, Fig. S2*B*). Tissue niches for MFs are typically seeded by embryonic precursors during fetal development and are later filled by bone marrow (BM)-derived monocytes (33). Given the potentially distinct ontogeny of the early perinatal MMs, we wondered how their differentiation trajectories might differ from those of older mice. Thus, we distilled out the MM population at the two ages and reclustered it (*SI Appendix*, Fig. S3*B*). RNA-velocity analysis revealed that, regardless of age, putative MM trajectories suggested differentiation toward *Ly6c2*- MM populations over time (Fig. 3*E* and *SI Appendix*, Fig. S3 *C* and *D*). This observation was partially in line with the expected differentiation pathway of circulating MM once within tissues; however, it was surprising to observe the mature cells (MHCII$^+$ MM or *Mertk*$^+$ MM) showing putative differentiation trajectories toward the *Ly6c2*- MM populations (34). Histograms of MM proportions over time further suggested a D5-LN environment rich in MHCII$^+$ and a shift toward the *Ly6c*- population by W2 (Fig. 3*F*).

These observations were orthogonally validated via flow cytometry, confirming that the Ly6C^{hi} to Ly6C^{lo} ratio decreased over time (*SI Appendix*, Fig. S3*E*, gating schema in *SI Appendix*, Fig. S2*B*). Principal component analysis (PCA) of population-level RNAseq of sorted LN Ly6C^{hi} and Ly6C^{lo} MM from mice of the two ages showed these populations to segregate by both Ly6C state and age (*SI Appendix*, Fig. S3*F*). Capturing just the age-related component revealed a broad shift from proliferation and growth pathways (e.g., "Myc Targets," "EM transition," "Cholesterol homeostasis") at D5 to inflammatory signaling pathways (e.g., "Interferon signaling," "Antigen processing and presentation") by W2 (*SI Appendix*, Fig. S3 *G* and *H*). Overall, these findings suggest an LN APC environment that increases in inflammatory tone over time.

Lymphocyte Waves in the LN. In the mouse, waves of lymphocytes progressively seed the LN during fetal and postnatal development. Lymphoid tissue inducer (LTi) cells, a subtype of type 3 innate lymphoid cells (ILC3s), first seed LNs at embryonic day 12–17, soon followed by waves of other innate and invariant lymphocytes, such as gamma-delta T (Tγδ) cells (35, 36). The first Tαβ cells arrive in the

LN at birth and fill the niche through homeostatic proliferation (37). To assess the heterogeneity of early lymphocytes across the perinatal window, we distilled and reclustered the lymphocyte constituents of the scRNAseq data illustrated in Fig. 1*A* and labeled the major cell types according to expression of key marker genes and cell-type signatures (Fig. 4 *A* and *B*). The innate and invariant lymphocyte clusters segregated primarily according to expression of the core TFs *Rorc* and *Tbx21*, with ILC1s and *Tbx21*$^+$ Tγδ coclustering apart

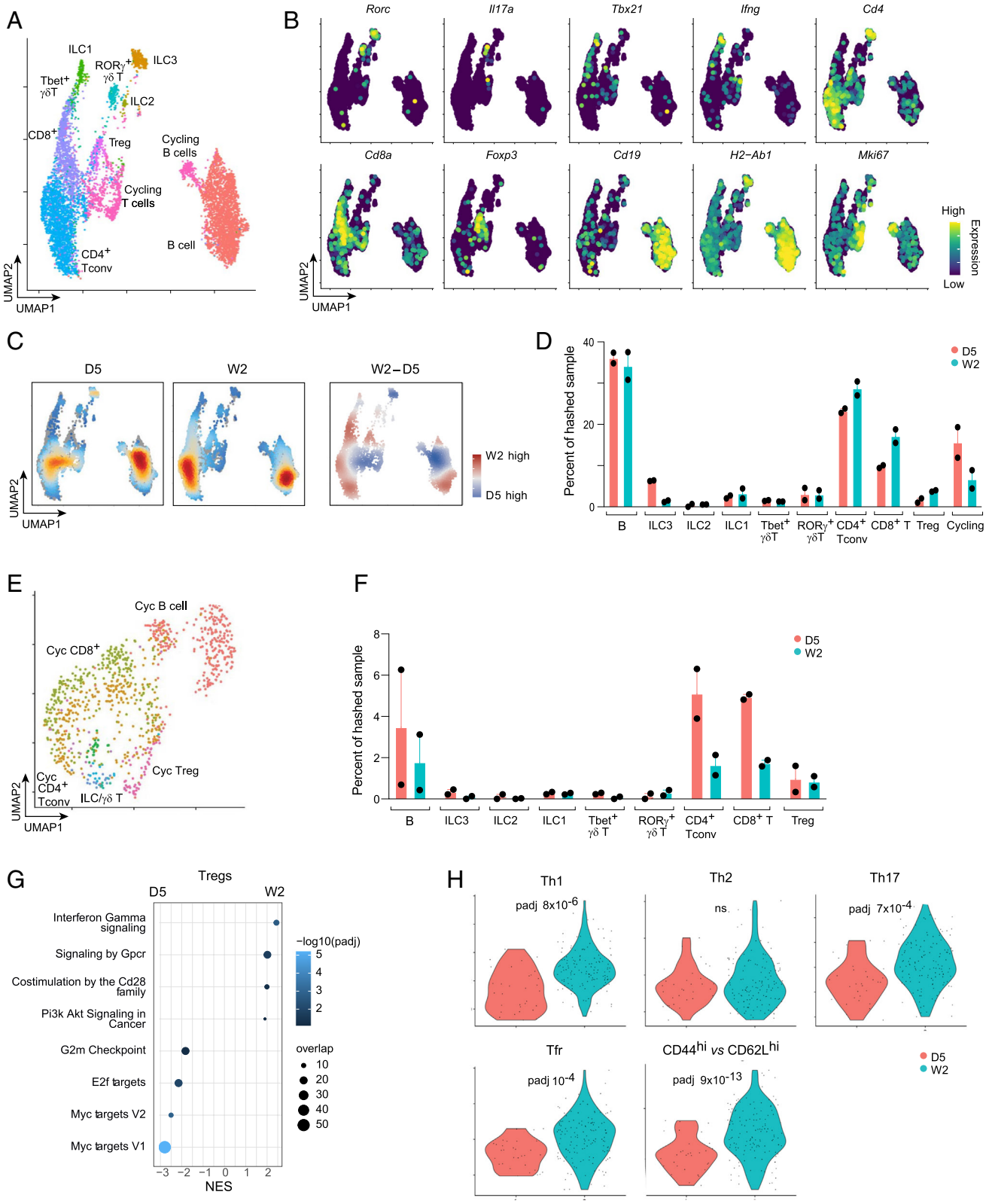

Fig. 4. Lymphocytes populate the early lymph node. (*A*) UMAP plot of D5 and W2 lymphocyte populations. (*B*) UMAP plot as in *A* colored by the scaled expression of each indicated gene. (*C*) Local cell densities of (*Left*) D5, (*Middle*) W2, and (*Right*) density differential. (*D*) Proportion of subtype cluster per age. (*E*) UMAP plot of cycling lymphocytes. (*F*) Proportion of each cycling lymphocyte subtype cluster per age. (*G*) Relevant GSEA plots of W2 vs. D5 Treg transcripts. (*H*) Gene signature scores of Tregs from D5 and W2. Signature significance p-adjusted value calculated through GSEA. Th, T helper; Tfr, follicular regulatory T cells; other abbreviations as in Fig. 1.

from ILC3s and *Rorc*$^+$ Tγδ cells (Fig. 4*B*). Segregation of the Tγδ populations coincided with the two age-restricted waves known to populate the LN: IL17$^+$ Tγδ cells (*Il17a*$^+$*Rorc*$^+$) were generated exclusively during fetal and perinatal development while their IFNγ$^+$ counterparts (*Ifng*$^+$*Tbx21*$^+$) were made postnatally (36, 38) (Fig. 4*B*). There was an enrichment for ILC3s and cycling T and B cells during the first week of life, followed by a shift to noncycling canonical lymphocyte types: *Cd8*$^+$ T cells, *Cd4*$^+$ conventional T cells (Tconv), and *Foxp3*$^+$ Tregs, as well as increased MHCII transcript expression by B cells (Fig. 4 *B*–*D*). Reclustering the cycling cells revealed the increased division at D5 to be driven predominantly by cycling CD4$^+$ Tconv, CD8$^+$ T and B cells (Fig. 4 *E* and *F*).

Given the importance of the perinatal Treg wave in tissue tolerance, we wondered what unique transcriptional programs might be expressed during the perinatal window. GSEA comparing noncycling Tregs across the perinatal window revealed D5 Tregs to be enriched for pathways associated with proliferation and growth, such as "Myc targets" and "E2F targets" (Fig. 4*G* and *SI Appendix*, Fig. S4*A*). By W2, Tregs preferentially expressed genes involved in activation and inflammation pathways, such "IFNγ signaling" and "costimulation by the CD28 family" (Fig. 4*G* and *SI Appendix*, Fig. S4*B*). W2 Tregs were also enriched for published signatures of T-helper subtypes (Th1, Th17, and Tfr, but not Th2) and activation (CD44^{Hi}vsCD62L^{Hi}) (Fig. 4*H*). It has previously been reported that the Treg compartment can include subtypes that mirror the type of immune responses they are regulating (39).

The LN Stromal Cell Response to T Cell Dysregulation. The above observations on the perinatal niche in wild-type (WT) mice argued for a dynamic stromal cell compartment predicted to have abundant interactions with the first wave of Tαβ cells. In the thymus, stromal cell cross talk with maturing T cells is essential for their differentiation (40, 41). Likewise, cross talk between LTi cells and the mesenchymal stromal cell precursors called lymphoid-tissue organizer (LTo) cells drives early LN organogenesis (35). Hence, we wondered whether the emergence of new stromal cell subtypes between D5 and W2 (Fig. 2 *D* and *E*) was influenced by the arrival of Tαβ populations in the LN. To address this point, we examined TCRβ-deficient mice, which lack Tαβ cells in the periphery due to arrested differentiation in the thymus, but have robust ILC, Tγδ cell, and B cell compartments (42). Peripheral LNs from *Trb*$^{wt/wt}$ (TCRβ-WT) and *Trb*$^{tm1Mom/tm1Mom}$ (TCRβ-KO) littermates were profiled as above using scRNAseq (*SI Appendix*, Fig. S5*A*). The LNs from TCRβ-KO mice had all of the expected cell populations (As per Fig. 1*A*), lacking only Tαβ cells (*SI Appendix*, Fig. S5 *A* and *B* and Fig. 1*A*).

Distillation of the FRCs from D5 and W2, followed by reclustering, yielded the expected 5 subtypes, according to marker-gene expression (Fig. 5*A*, as per Fig. 2*C*). One of the most prominent changes in response to the loss of Tαβ cells occurred on D5, when stromal cells from TCRβ-KO mice had a lower proportion of cells in cycle (Fig. 5 *B* and *C*). Histograms of cycling cells demonstrated the reduction in TCRβ-KO mice on D5 to be largely driven by a preferential loss of cycling *Ccl19*$^+$/*Cxcl12*$^+$ subtypes, although *Cd34*$^+$ cells also cycled substantially less (*SI Appendix*, Fig. S5*C*). By W2, there was a global decrease in the cycling stromal cells, which muted the preferential decline in cycling *Ccl19*$^+$/*Cxcl12*$^+$ and *Cd34*$^+$ subtypes in TCRβ-KO mice.

Beyond the differences in proportions of cycling cells, loss of Tαβ cells resulted in clear density shifts within the *Ccl19*$^+$ noncycling subtype at D5 and W2 (Fig. 5*B*), pointing to transcriptional changes. GSEA analysis of differential gene expression highlighted inflammation-related pathways in both cases (Fig. 5 *D* and *E*). There was also clear upregulation of the signature of activated Nr4a1$^+$ LN stromal cells in D5 TCRβ-KO mice (Fig. 5*F*) (30, 43). *Cd34*$^+$ populations and PvCs also showed upregulation of inflammatory pathways predominantly at D5 (*SI Appendix*, Fig. S5*D*) but also at W2 (*SI Appendix*, Fig. S5*E*).

As a complement, we performed an analogous study on the effects of an influx of autoreactive T cells. Specifically, we looked at the D5-W2 window in Aire-deficient mice, which have a general defect in thymic tolerance induction, culminating in multi-organ autoimmunity (14). Notably, when the *Aire*-null mutation is carried on the B6 background, disease is well controlled into adulthood, with tissue infiltration usually detected only after 8 wk of age. Furthermore, this model of autoreactivity is especially sensitive to the perinatal period (15, 16), allowing us to probe early responses to autoreactive T cells while minimizing secondary inflammatory responses.

scRNAseq profiling of LN cells from 5D and W2 Aire-WT and Aire-KO female littermates revealed the expected populations (*SI Appendix*, Fig. S5 *F* and *G*; cf Fig. 1*A*). From the complete dataset, we distilled the FRC compartment of both genotypes and ages, reclustered them, and used key marker genes to annotate broad stromal subclusters (Fig. 5*G*). As with the TCRβ-WT/-KO comparison, there were changes in the *Ccl19*$^+$ subtype in the Aire-deficient mice, especially at D5 (Fig. 5 *H* and *I*). At that time point, there were also changes in representation of the PvC and *Cd34*$^+$ subtypes at D5 in Aire-KO mice, which had normalized by W2. Pathway analysis via GSEA revealed that, already at D5 but more so at W2, pathways related to the inflammatory response were increased in Aire-KO mice—e.g., "Abnormal inflammatory response" or "Cell activation involved in Immune response" at D5 and "Interferon gamma response" or "Innate immune response" at W2 (Fig. 5 *J* and *K*). Overall, the cellular and transcriptional shifts suggested that the stroma could sense and respond to changes in the T cell compartment even as early as D5.

Treg-Dependent Stromal Cell Activation. Both the absence of T cells in TCRβ-KO mice and the presence of autoreactive T cells in Aire-KO mice provoked an increase in transcriptional pathways associated with cell activation and inflammatory responses. Common to the two models is a deficiency in Treg cells: a complete absence in the context of total Tαβ cell deficiency and a defect in perinatal Tregs in the context of Aire deficiency (16). Thus, we hypothesized that Treg dysregulation might underlie stromal cell activation in the two models.

To explore the role Tregs might play in keeping stromal cell activation in check, we punctually depleted them via diphtheria toxin (DT) treatment of mice expressing the DT receptor (DTR) specifically in Foxp3$^+$ cells (B6.Foxp3^{DTR} mice) (44). Focusing on the perinatal response to Treg depletion, we exposed D3-5 perinates to a 3-d course of DT (Fig. 6*A*), which efficiently blocked Tregs 3 and 6 d after the first injection, followed by their recovery—even overshoot—fourteen days postinjection (Fig. 6*B*). In line with our hypothesis, loss of Tregs precipitated stromal cell activation, measured cytometrically as Sca1 display (45, 46) (Fig. 6*C*, gating schema in *SI Appendix*, Fig. S2*A*). Interestingly, stromal cell activation was evident beyond the time point when Treg numbers had recovered. Conventional CD4$^+$ T cells were also activated, with a time course similar to that of stromal cells (Fig. 6*D*).

Since one of the initial effects of Treg loss in a number of systems is the unleashing of interferon-gamma (IFNγ) production (47–49), we asked whether the increase in LN Sca1$^+$ FRCs after perinatal Treg depletion was driven by IFNγ signaling. First, in a gain-of-function experiment, we ip-injected 3–5-d-old B6 mice with recombinant IFNγ (rIFNγ) or phosphate-buffered-saline (PBS) over a 1-wk period and assayed FRC activation on the next

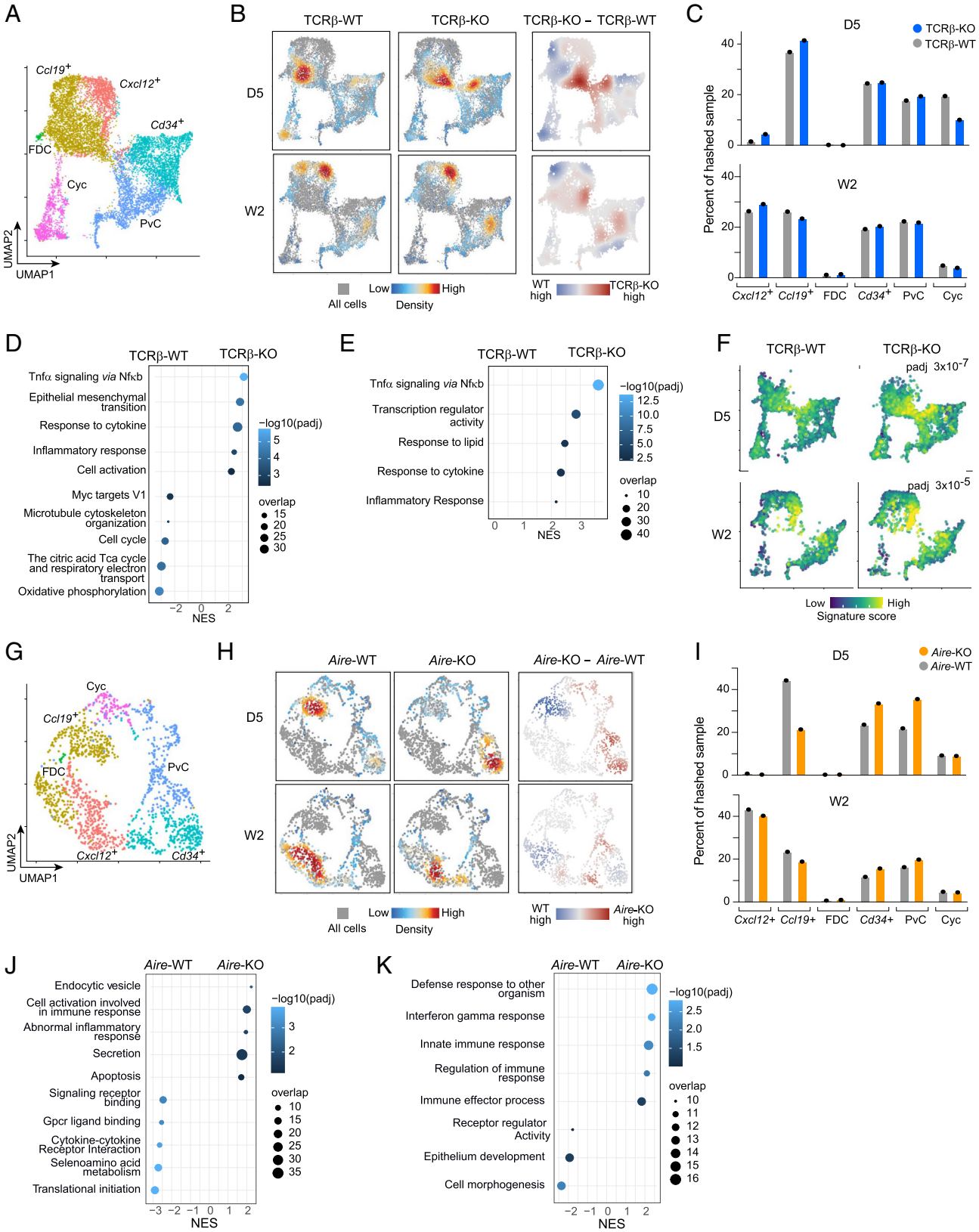

Fig. 5. Stromal cell response to T cell dysregulation. (*A*) UMAP plot of TCRβ-WT and -KO populations from D5 and W2 colored by the FRC subpopulation clusters. (*B*) Local cell densities (*Left* and *Middle*) and density differential plots (*Right*) as in Fig. 2. (*C*) Proportion of stromal subtypes by age. (*D*) Relevant GSEA plots of noncycling D5 *Ccl19*+FRC transcripts in TCRβ-KO vs. -WT. (*E*) As in panel *D*, comparing W2 TCRβ-KO vs. -WT. (*F*) UMAP plot as in *A* Signature scores for "*Nr4a1*+ stromal cell" overlain on the FRCs UMAP of Fig. 5*B*. (*G*) UMAP plot of Aire-WT and -KO populations from D5 and W2. (*H*) Local cell densities (*Left* and *Middle*) and density differential plots (*Right*). (*I*) Proportion of stromal subtypes by age. (*J*) GSEA plots D5 noncycling FRCs at D5 Aire-KO vs. -WT. (*K*) Relevant GSEA plots as in *J*, but for W2 Aire-KO vs. -WT.

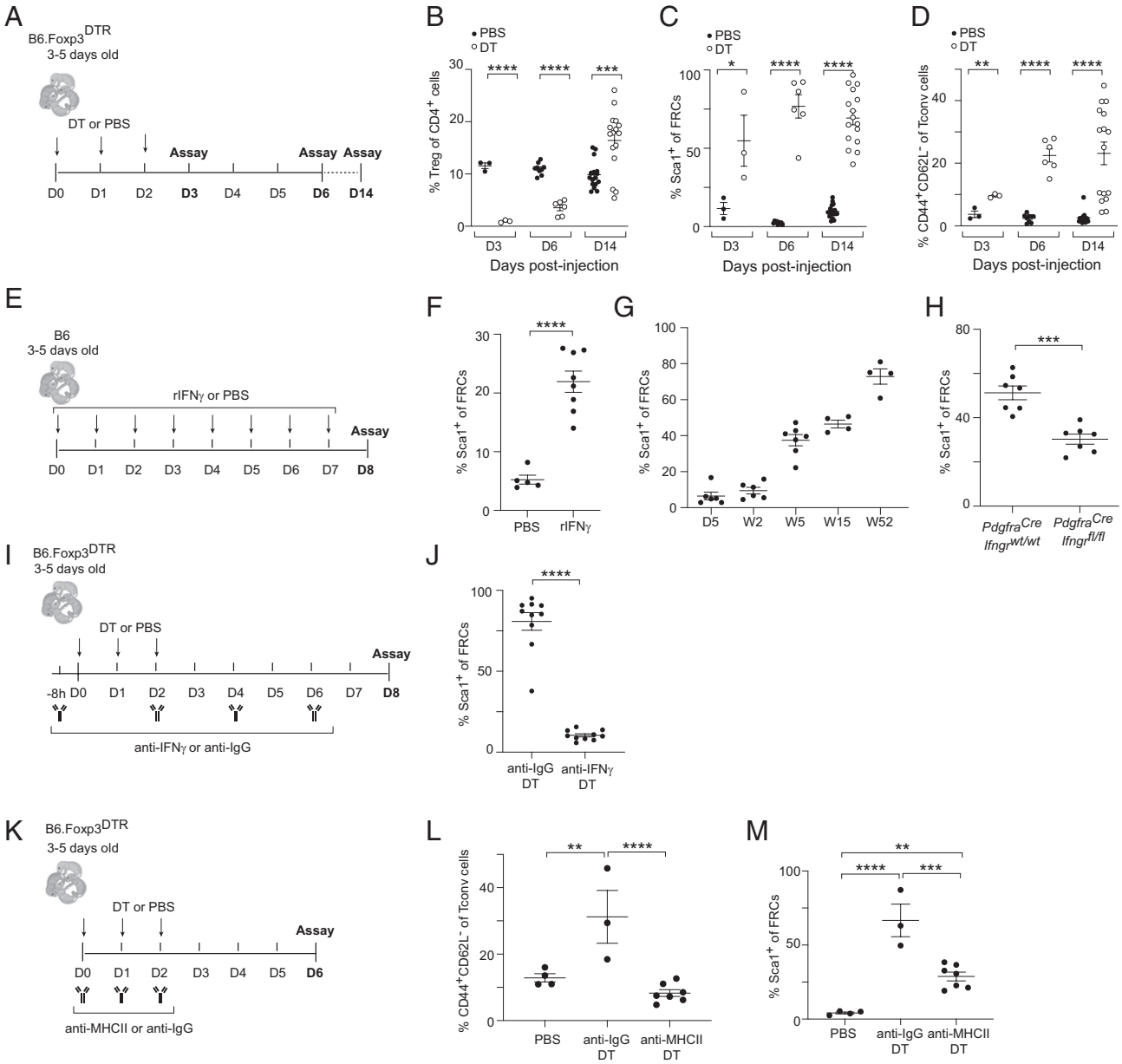

Fig. 6. Impact of Treg cell and IFNγ dysregulation on stromal cells. (*A*) Schematic of Treg depletion protocol. Summarized flow cytometry data for (*B–D*) treatment schedule as in *A*. (*B*) Foxp3+Tregs as a percent of total CD4+ T cells; (*C*) Sca1+FRCs as a percent of total FRCs cells; (*D*) CD44+CD62L- Tconv as a percent of total Tconv cells. (*E*) Schematic of rIFNγ administration protocol. (*F*) Summarized data from treatment schedule (*E*) of Sca1+FRCs as a percent of total FRCs. (*G*) Quantification of Sca1+FRCs as a percent of total FRCs in B6 WT LN across time. (*H*) Quantification of Sca1+FRCs as a percent of total FRCs in aged 12–20 wk old *Pdgfra*^{Cre}*Ifngr1*$^{wt/wt}$ vs. *Pdgfra*^{Cre}*Ifngr1*$^{fl/fl}$ mice. (*I*) Schematic of IFNγ blockade protocol. (*J*) Treatment schedule as in *I*, Sca1+FRCs as a percent of total FRCs. (*K*) Schematic of MHC-II blockade protocol. (*L*) Treatment schedule as in *K*, Quantification of CD44+CD62L- Tconv as a percent of total Tconv cells. (*M*) Quantification of Sca1+FRCs as a percent of total FRCs cells. For all flow cytometry quantification plots above, each dot represents an independent mouse, data were pooled from two to five independent experiments, *P* values were calculated by two-sided unpaired Student's *t* test for *B*, *C*, *D*, *F*, and *H* and one-way ANOVA for *L* and *M*, and bars represent mean ± SEM. N = 3 to 18; as indicated. DT, diphtheria toxin; PBS, phosphate-buffered saline; D, day; rIFNγ, recombinant interferon gamma; MHCII, class II major histocompatibility molecule; IgG, immunoglobulin isotype G.

day by flow cytometry (Fig. 6*E*). The rIFNγ-injected mice had four to five times more Sca1$^+$ FRCs than did their PBS-injected littermates (Fig. 6*F*). Interestingly, the increase in activated FRCs was reminiscent of a physiological age-associated rise in Sca1$^+$ FRCs, with less than 20% of unmanipulated perinatal FRCs displaying Sca1, a fraction that continuously rose to over 60% by 1 y of age (Fig. 6*G*). IFNγ-induced FRC activation was primarily a direct effect because it occurred to a much lower degree in aged mice lacking the receptor for IFNγ specifically on PDGFRα$^+$ stromal cells (referred to as *Pdgfra*^{Cre}x *Ifngr1*$^{fl/fl}$) (Fig. 6*H*). The partial effect of IFNGR1 deletion might reflect either incomplete deletion of the receptor or some participation by other cell types.

We also performed loss-of-function experiments. Sustained neutralization of IFNγ throughout the course of Treg depletion plus an additional week post-DT treatment (Fig. 6*I*) almost abrogated the increase in Sca1$^+$ FRCs (Fig. 6*J*). Thus the FRC activation induced by the loss of Tregs was driven by IFNγ. Last, we established that the FRC activation was not entirely a direct effect of their loss of exposure to Tregs. Concurrent depletion of Tregs with DT and inhibition of Tconv cell activation with an antibody recognizing MHCII molecules (Fig. 6 *K* and *L*) argued that stromal cell activation was also partly dependent on TCR:MHC–peptide interactions and activation of Tconv cells (Fig. 6*M*). Thus, the presence of perinatal Tregs helped assure LN stromal cell

homeostasis through control of IFNγ signaling and bystander CD4$^+$ Tconv cell activation.

Discussion

The first 2 wk of life are essential for the establishment of lifelong T cell tolerance because a unique wave of tissue-protective Tregs is engendered and Tconv cells accessing tissues are converted to an anergic phenotype during this period (16, 27). We asked what cellular environment T cells encounter in the LNs upon their initial emergence from the thymus and how that environment evolves over the next days. Our findings highlight dynamic cellular and transcriptional shifts between D5 and W2—in particular in the stromal cell compartment, which evolved from a cycling to an immunocyte-promoting state. Across the predominant non-stromal compartments—APCs and lymphocytes—there was a shift from growth and cell cycling at D5 toward activation and inflammatory signaling at W2. Examination of mouse perinates lacking all Tαβ cells or enriched in autoreactive Tαβ cells demonstrated perinatal stromal cells to be highly sensitive to T cell dysregulation, reflecting at least partly Treg and, consequently, IFNγ dysregulation.

The promotion of novel LN stromal cell subtypes with the immigration of T cells mirrored LTi-LTo interactions reported to drive fetal LN development (35). Congruent with a role for T cell cross talk in stromal cell differentiation, Tαβ deficiency also led to a decline in proliferation, specifically of cycling cells bearing markers of T-zone reticular cells, such as the *Ccl19*$^+$ subtype. However, this transcriptional shift could not explain the magnitude of stromal cell shifts across time. Instead, two broad possibilities exist. First, while LTi-LTo cross talk is essential for LN formation, especially through RANK and lymphotoxin signaling (50, 51), Tαβ cell cross talk may play a more subtle role in postnatal LN differentiation. Alternatively, loss of Tαβ cells—especially Tregs—may have induced compensatory responses through dysregulation of other LN residents, such as Tγδ cells and ILCs. Evidence in support of a compensatory response may be in the signatures for activation or elevated inflammatory signaling pathways observed in TCRβ-KO stromal cells. Highlighting the sensitivity of stromal cells to loss of T cell homeostasis, exposure of stromal cells to an autoreactive T cell repertoire in Aire-deficient mice similarly featured transcriptional signs of activation and an IFNγ response.

Strong support for perinatal stromal cell sensitivity to T cell dysregulation came from mice wherein Tregs were punctually depleted perinatally, with their stromal cell activation dependent on both IFNγ and Tconv cell activation. This observation is in line with multiple studies showing a role for Tregs in controlling IFNγ responses (47–49). For example, punctual depletion of Tregs in autoimmunity-prone NOD mice promoted activation of and IFNγ production by Tconv and NK cells (48). Likewise, survival in *scurfy* mice, which are Treg-deficient from birth, is improved through null mutations in the signaling pathways related to type 1 immune responses, e.g., *Ifngr1* or *Tbx21* mutations (49).

Given the role of Tregs in setting the IFNγ tone in perinatal LNs, the long-term impact of stromal responses to early inflammatory signals remains to be explored. Stromal cells have been implicated in tolerance induction, including through IFNγ-induced MHCII or PD-L1 expression (5). It is possible that the inflammatory tone of the perinatal LN environment, here observed through dysregulation of Tregs and/or IFNγ production, may lead to divergent differentiation pathways for stromal cell subsets that induce or inhibit T cell activation. For example, in our study of stromal cells in Aire-deficient mice, there was also an acute decrease in T-zone reticular cell–like *Ccl19*$^+$ populations at D5, which may temper T cell activation through dampening interactions between CCR7$^+$ cells such as naive T cells and DCs. Together this potential for LN remodeling as stromal cells respond to the inflammatory tone of the early LN environment poses a unique synergy with Tregs for modulating T cell responses.

Materials and Methods

Mice. All mice were maintained in accordance with Harvard Medical School's Animal Care and Use Committee guidelines (IACUC protocol #IS00001257). TCRβ-KO (B6.129P2-*Tcrb*^{tm1Mom}/J, JAX #002118), Aire-KO (52), *Foxp3*^{DTR} (B6.*Foxp3*^{DTR}, from A. Rudensky at Memorial Sloan Kettering Cancer Center, New York, NY) (53), *Ifngr1*$^{fl/fl}$ (*Ifngr*$^{tm1.1Rds}$/J, JAX #025394), and *Pdgfra*^{Cre} (Tg(Pdgfra-Cre)1Clc/J JAX #013148) (54) mice were all maintained on a B6 background. Mice lacking IFNGR1 on stromal cells were generated by crossing *Pdgfra*^{Cre} with *Ifngr1*^{fl} mice. Female littermates were used for all transcriptomic experiments.

Mouse Treatments. Tregs were ablated in B6.*Foxp3*$^{DTR+/+}$ littermates aged 3 to 5 d old via ip injection of DT (Sigma) at 20 ng/g body weight or phosphate-buffered saline (PBS) for three consecutive days. Concurrent in vivo IFNγ ablation was accomplished using 10 μg/g rat Ultra-LEAF purified anti-mouse IFNγ monoclonal antibody (mAb) (clone XMG1.1, BioLegend) or the IgG1κ-isotype control (clone RTK2071, BioLegend). Perinatal mice were ip-injected with antibody 8 h before the first DT injection, followed by antibody treatment on D2, D4, and D6 post-DT injection. DT and antibody were coinjected on D2 to minimize perinatal stress. Concurrent MHCII blockade was achieved using 20 μg/g anti-mouse I-A/I-E (clone M5/114, InVivoMAb), or rat IgG2b control (clone LTF-2, InVivoMAb), ip-injected with DT for three consecutive days.

For gain-of-function in vivo cytokine injections, rIFNγ or PBS control were ip-injected into 3 to 5-d-old B6 perinates with 100 ng/g body weight daily for eight consecutive doses starting on D0 and ending on D7.

Cell Isolation and Flow Cytometry. Pooled perinatal inguinal, axillary, and brachial LNs were dissected under the microscope and collected in 2-mL Eppendorf tubes containing 1 mL sterile RPMI with 2% fetal bovine serum (FBS). LNs were digested using a protocol modified from ref. 55 to capture both hematopoietic and nonhematopoietic cells. Further details on cell isolation and analysis in *SI Appendix, Materials and Methods*.

scRNAseq and Analysis. Pooled LNs were isolated from female WT and KO littermates aged D4-6, D12-15, and D30-45. Each replicate was processed, encapsulated, and sequenced independently. Samples were gently digested and cytofluorometrically sorted according to CD45.2 expression and encapsulated using the Chromium Single cell 3′ v3 (10× Genomics).

Data were processed using the standard cellranger pipeline (10× Genomics). Downstream analysis was performed using the Seurat v4 pipeline (56). Velocity analysis was conducted using the scVelo package (57). Cell-interaction networks were constructed using the cellchat package (29). Further information related to data analysis can be found in *SI Appendix, Materials and Methods*.

Population-Level RNA-seq Library Preparation and Sequencing. Flow cytometrically purified cell populations ranging from 500 to 1,000 cells were double-sorted for each replicate. Library preparation was conducted using the Smart-seq2 RNA-seq protocol. Sequencing was conducted at the Broad Genomics Platform following the standard Immgen (https://www.immgen.org). Further information on data processing and quality control can be found in *SI Appendix, Materials and Methods*.

Gene Signatures. The stromal cell activation signature was computed on the basis of the differentially expressed genes in *Nr4a1*+ LN stromal cells found in ref. 30, with further filtering of genes [fold-change > 2 and false discovery rate (FDR) < 0.05]. Th1, Th2, and Th17 signatures from ref. 58 CD44+CD62L- Treg signature from ref. 59 and Tfh signature from ref. 60.

Statistics. For pathway and signature analyses, GSEA was used with the Benjamini–Hochberg method for *P*-value adjustment. Flow cytometry data are shown as mean ± SEM. Unless otherwise stated, statistical significance was determined using Student's *t* test or ANOVA using GraphPad Prism 9.0. $*P < 0.05$, $**P < 0.01$, $***P < 0.001$, and $****P < 0.0001$.

Data, Materials, and Software Availability. Single-cell RNA-seq and population RNA-seq data have been deposited in GEO (GSE244743) (61). All other data are included in the manuscript and/or *SI Appendix*.

ACKNOWLEDGMENTS. We thank M. Marin-Rodero, D. Michelson, O. K. Yaghi, P. K. Langston, T. Xiao, A. Mann, V. Piekarsa, R. G. Spallanzani, A. Muñoz-Rojas, and G. Wang for experimental assistance and insightful discussion; K. Seddu, A. Baysoy, J. Lee, I. Magill, and the Broad Genomics Platform for RNAseq; L. Yang, B. Vijaykumar, N. Patel, D. Zemmour, and D. Mallah for computational assistance; and D. Ischiu, C. Araneo, M. Sleeper, and J. Nelson from Harvard Medical School's Immunology Flow Cytometry Core. This work was supported by NIH grant DK060027 to D.M. and NIH Training Grant Numbers T32GM007753 and T32GM144273 to T.J.

1. M. Irla, Instructive cues of thymic T cell selection. *Annu. Rev. Immunol.* **40**, 95–119 (2022).
2. L. Klein, B. Kyewski, P. M. Allen, K. A. Hogquist, Positive and negative selection of the T cell repertoire: What thymocytes see (and don't see). *Nat. Rev. Immunol.* **14**, 377–391 (2014).
3. D. L. Mueller, Mechanisms maintaining peripheral tolerance. *Nat. Immunol.* **11**, 21–27 (2010).
4. M. A. ElTanbouly, R. J. Noelle, Rethinking peripheral T cell tolerance: Checkpoints across a T cell's journey. *Nat. Rev. Immunol.* **21**, 257–267 (2021).
5. A. T. Krishnamurty, S. J. Turley, Lymph node stromal cells: Cartographers of the immune system. *Nat. Immunol.* **21**, 369–380 (2020).
6. R. H. Schwartz, Historical overview of immunological tolerance. *Cold Spring Harb. Perspect. Biol.* **4**, a006908 (2012).
7. J. Lederberg, Genes and antibodies. *Science* **129**, 1649–1653 (1959).
8. T. Forsthuber, H. C. Yip, P. V. Lehmann, Induction of T_H1 and T_H2 immunity in neonatal mice. *Science* **271**, 1727–1730 (1996).
9. N. Chen, E. H. Field, Enhanced type 2 and diminished type 1 cytokines in neonatal tolerance. *Transplantation* **59**, 933–941 (1995).
10. R. R. Singh, B. H. Hahn, E. E. Sercarz, Neonatal peptide exposure can prime T cells and upon subsequent immunization, induce their immune deviation: Implications for antibody vs. T cell-mediated autoimmunity. *J. Exp. Med.* **183**, 1613–1621 (1996).
11. J. P. Ridge, E. J. Fuchs, P. Matzinger, Neonatal tolerance revisited: Turning on newborn T cells with dendritic cells. *Science* **271**, 1723–1726 (1996).
12. M. Sarzotti, D. S. Robbins, P. M. Hoffman, Induction of protective CTL responses in newborn mice by a murine retrovirus. *Science* **271**, 1726–1728 (1996).
13. K. S. Tung *et al.*, Autoimmune ovarian disease in day 3-thymectomized mice: The neonatal time window, antigen specificity of disease suppression, and genetic control. *Curr Top. Microbiol. Immunol.* **293**, 209–247 (2005).
14. M. S. Anderson *et al.*, Projection of an immunological self shadow within the thymus by the aire protein. *Science* **298**, 1395–1401 (2002).
15. M. Guerau-de-Arellano, M. Martinic, C. Benoist, D. Mathis, Neonatal tolerance revisited: A perinatal window for Aire control of autoimmunity. *J. Exp. Med.* **206**, 1245–1252 (2009).
16. S. Yang *et al.*, Regulatory T cells generated early in life play a distinct role in maintaining self-tolerance. *Science* **348**, 589–594 (2015).
17. S. Gilfillan *et al.*, Mice lacking TdT: Mature animals with an immature lymphocyte repertoire. *Science* **261**, 1175–1178 (1993).
18. T. Komori, A. Okada, V. Stewart, F. W. Alt, Lack of N regions in antigen receptor variable region genes of TdT-deficient lymphocytes. *Science* **261**, 1171–1175 (1993).
19. M. A. Gavin, M. J. Bevan, Increased peptide promiscuity provides a rationale for the lack of N regions in the neonatal T cell repertoire. *Immunity* **3**, 793–800 (1995).
20. K. Ikuta *et al.*, A developmental switch in thymic lymphocyte maturation potential occurs at the level of hematopoietic stem cells. *Cell* **62**, 863–874 (1990).
21. L. A. Herzenberg, L. A. Herzenberg, Toward a layered immune system. *Cell* **59**, 953–954 (1989).
22. D. E. Harrison *et al.*, Relative to adult marrow, fetal liver repopulates nearly five times more effectively long-term than short-term. *Exp. Hematol.* **25**, 293–297 (1997).
23. A. W. Goldrath *et al.*, The molecular program induced in T cells undergoing homeostatic proliferation. *Proc. Natl. Acad. Sci. U.S. A.* **101**, 16885–16890 (2004).
24. J. E. Park *et al.*, A cell atlas of human thymic development defines T cell repertoire formation. *Science* **367**, eaay3224 (2020).
25. J. Pezoldt *et al.*, Neonatally imprinted stromal cell subsets induce tolerogenic dendritic cells in mesenteric lymph nodes. *Nat. Commun.* **9**, 3903 (2018).
26. J. Pezoldt *et al.*, Postnatal expansion of mesenteric lymph node stromal cells towards reticular and $CD34^+$ stromal cell subsets. *Nat. Commun.* **13**, 7227 (2022).
27. J. Tuncel, C. Benoist, D. Mathis, T cell anergy in perinatal mice is promoted by T reg cells and prevented by IL-33. *J. Exp. Med.* **216**, 1328–1344 (2019).
28. J. M. Gardner, A. Liston, RORγt-lineage APCs: The Aire apparent. *Sci. Immunol.* **7**, eade9240 (2022).
29. S. Jin *et al.*, Inference and analysis of cell-cell communication using Cell Chat. *Nat. Commun.* **12**, 1088 (2021).
30. L. B. Rodda *et al.*, Single-cell RNA sequencing of lymph node stromal cells reveals niche-associated heterogeneity. *Immunity* **48**, 1014–1028 (2018).
31. L. B. Rodda *et al.*, Phenotypic and morphological properties of germinal center dark zone Cxcl12-expressing reticular cells. *J. Immunol.* **195**, 4781–4791 (2015).
32. L. Li *et al.*, Lymph node fibroblastic reticular cells steer immune responses. *Trends Immunol.* **42**, 723–734 (2021).
33. Y. Lavin, A. Mortha, A. Rahman, M. Merad, Regulation of macrophage development and function in peripheral tissues. *Nat. Rev. Immunol.* **15**, 731–744 (2015).
34. F. Ginhoux, S. Jung, Monocytes and macrophages: Developmental pathways and tissue homeostasis. *Nat. Rev. Immunol.* **14**, 392–404 (2014).
35. L. Onder, B. Ludewig, A fresh view on lymph node organogenesis. *Trends Immunol.* **39**, 775–787 (2018).
36. S. R. Carding, P. J. Egan, Gammadelta T cells: Functional plasticity and heterogeneity. *Nat. Rev. Immunol.* **2**, 336–345 (2002).
37. B. Min *et al.*, Neonates support lymphopenia-induced proliferation. *Immunity* **18**, 131–140 (2003).
38. I. Prinz, B. Silva-Santos, D. J. Pennington, Functional development of gd T cells. *Eur. J. Immunol.* **43**, 1988–1994 (2013).
39. A. G. Levine *et al.*, Stability and function of regulatory T cells expressing the transcription factor T-bet. *Nature* **546**, 421–425 (2017).
40. W. van Ewijk, E. W. Shores, A. Singer, Crosstalk in the mouse thymus. *Immunol. Today.* **15**, 214–217 (1994).
41. J. Abramson, E. S. Husebye, Autoimmune regulator and self-tolerance–Molecular and clinical aspects. *Immunol. Rev.* **271**, 127–140 (2016).
42. P. Mombaerts *et al.*, Mutations in T-cell antigen receptor genes alpha and beta block thymocyte development at different stages. *Nature* **360**, 225–231 (1992).
43. K. S. Ullman, J. P. Northrop, C. L. Verweij, G. R. Crabtree, Transmission of signals from the T lymphocyte antigen receptor to the genes responsible for cell proliferation and immune function: The missing link. *Annu. Rev. Immunol.* **8**, 421–452 (1990).
44. J. M. Kim, A. Rudensky, The role of the transcription factor Foxp3 in the development of regulatory T cells. *Immunol. Rev.* **212**, 86–98 (2006).
45. D. J. Izon *et al.*, Identification and functional analysis of Ly-6A/E as a thymic and bone marrow stromal antigen. *J. Immunol.* **156**, 2391–2399 (1996).
46. C. Perez-Shibayama *et al.*, Type I interferon signaling in fibroblastic reticular cells prevents exhaustive activation of antiviral $CD8^+$ T cells. *Sci. Immunol.* **5**, eabb7066 (2020).
47. M. Panduro, C. Benoist, D. Mathis, T_{reg} cells limit IFN-g production to control macrophage accrual and phenotype during skeletal muscle regeneration. *Proc. Natl. Acad. Sci. U.S.A.* **115**, E2585–E2593 (2018).
48. M. Feuerer *et al.*, How punctual ablation of regulatory T cells unleashes an autoimmune lesion within the pancreatic islets. *Immunity* **31**, 654–664 (2009).
49. T. J. Suscovich, N. R. Perdue, D. J. Campbell, Type-1 immunity drives early lethality in scurfy mice. *Eur. J. Immunol.* **42**, 2305–2310 (2012).
50. W. C. Dougall *et al.*, RANK is essential for osteoclast and lymph node development. *Genes Dev.* **13**, 2412–2424 (1999).
51. P. De Togni *et al.*, Abnormal development of peripheral lymphoid organs in mice deficient in lymphotoxin. *Science* **264**, 667–669 (1994).
52. W. Jiang *et al.*, Modifier loci condition autoimmunity provoked by Aire deficiency. *J. Exp. Med.* **202**, 805–815 (2005).
53. J. M. Kim, J. P. Rasmussen, A. Y. Rudensky, Regulatory T cells prevent catastrophic autoimmunity throughout the lifespan of mice. *Nat. Immunol.* **8**, 191–197 (2007).
54. K. Roesch *et al.*, The transcriptome of retinal Muller glial cells. *J. Comp. Neurol.* **509**, 225–238 (2008).
55. V. Lukacs-Kornek *et al.*, Regulated release of nitric oxide by nonhematopoietic stroma controls expansion of the activated T cell pool in lymph nodes. *Nat. Immunol.* **12**, 1096–1104 (2011).
56. Y. Hao *et al.*, Integrated analysis of multimodal single-cell data. *Cell* **184**, 3573–3587 (2021).
57. V. Bergen *et al.*, Generalizing RNA velocity to transient cell states through dynamical modeling. *Nat. Biotechnol.* **38**, 1408–1414 (2020).
58. E. Kiner *et al.*, Gut $CD4^+$ T cell phenotypes are a continuum molded by microbes, not by T_H archetypes. *Nat. Immunol.* **22**, 216–228 (2021).
59. A. G. Levine, A. Arvey, W. Jin, A. Y. Rudensky, Continuous requirement for the TCR in regulatory T cell function. *Nat. Immunol.* **15**, 1070–1078 (2014).
60. W. Sungnak *et al.*, T follicular regulatory cell-derived fibrinogen-like protein 2 regulates production of autoantibodies and induction of systemic autoimmunity. *J. Immunol.* **205**, 3247–3262 (2020).
61. T. Jayewickreme, C. Benoist, D. Mathis, Lymph Node Stromal Cell Responses to Perinatal T Cell Waves, A Temporal Atlas. NCBI's Gene Expression Omnibus. https://www.ncbi.nlm.nih.gov/geo/query/acc.cgi?acc=GSE244743. Deposited 5 October 2023.